Apo-intermediate in the transport cycle of lactose permease (LacY)

M. Gregor Madej[a], Sonya N. Soro[a], and H. Ronald Kaback[a,b,c,1]

Departments of [a]Physiology and [b]Microbiology, Immunology, and Molecular Genetics, and [c]Molecular Biology Institute, University of California, Los Angeles, CA 90095

Edited* by Christopher Miller, Howard Hughes Medical Institute, Brandeis University, Waltham, MA, and approved August 29, 2012 (received for review June 29, 2012)

The lactose permease (LacY) catalyzes coupled stoichiometric symport of a galactoside and an H^+. Crystal structures reveal 12, mostly irregular, transmembrane α-helices surrounding a cavity with sugar- and H^+- binding sites at the apex, which is accessible from the cytoplasm and sealed on the periplasmic side (an inward-facing conformer). An outward-facing model has also been proposed based on biochemical and spectroscopic measurements, as well as the X-ray structure of a related symporter. Converging lines of evidence demonstrate that LacY functions by an alternating access mechanism. Here, we generate a model for an apo-intermediate of LacY based on crystallographic coordinates of LacY and the oligopeptide/H^+ symporter. The model exhibits a conformation with an occluded cavity inaccessible from either side of the membrane. Furthermore, kinetic considerations and double electron-electron resonance measurements suggest that another occluded conformer with bound sugar exists during turnover. An energy profile for symport is also presented.

membrane proteins | modeling | membrane transport | conformational change

The major facilitator superfamily (MFS) of membrane transport proteins represents the largest family of secondary transporters, with members from *Archaea* to *Homo sapiens* (1, 2). MFS proteins catalyze transport of a wide range of substrates, including amines, acids, amino acids, sugars, peptides, and antibiotics, in many instances, by transducing the energy stored in an H^+ electrochemical gradient into a concentration gradient of substrate. The lactose permease of *Escherichia coli* (LacY), which catalyzes the coupled transport of a galactopyranoside and an H^+ (galactoside/H^+ symport) (3–6), is arguably the most extensively studied member of the MFS (7, 8). Essentially all 417 amino acyl side chains in LacY have been mutagenized (9), and functional analyses of the mutants reveals that fewer than 10 side chains play a central role in the symport mechanism (Fig. 1 *A* and *B*): Glu126 (helix IV), Arg144 (helix V), and Trp151 (helix V) are directly involved in galactoside recognition and binding; Tyr236 (helix VII), Glu269 (helix VIII), and His322 (helix X) are involved in both H^+ translocation and affinity for sugar; and Arg302 (helix IX) and Glu325 (helix X) play important roles in H^+ translocation (7, 10). In the available inward-facing crystal structures of LacY (11–14), these residues are located at the apex of a deep central hydrophilic cavity, which is open to the cytoplasm only (Fig. 1 *A* and *B*). The cavity is formed by 12 mostly irregular transmembrane helices organized in two pseudosymmetrical 6-helix bundles (helices I–VI and helices VII–XII) (11–14).

A six-step kinetic model for lactose/H^+ symport has been proposed (15, 16) (Fig. 1*C*). The steps include (*i*) deprotonation of LacY, (*ii*) a conformational change allowing the galactoside- and H^+-binding sites to become accessible to the other side of the membrane, (*iii*) protonation of LacY, (*iv*) substrate binding, (*v*) a global conformational change in which the protonated LacY with bound sugar returns to the initial inward-facing conformation, and (*vi*) dissociation of sugar. This sequence of events represents an alternating access mechanism in which the galactoside- and H^+-binding sites are exposed alternatively to either side of the membrane as a result of reciprocal opening and closing periplasmic and cytoplasmic cavities (8). Despite intense efforts, crystals of LacY have not yet been obtained in any conformation other than the inward-facing conformation. However, FucP, a distantly related MFS member, has been crystallized in an outward-facing conformation (17) that agrees well with models proposed for the outward-facing conformer of LacY (11, 18, 19).

On one hand, the outward-facing model clearly represents a distinct conformation, and individual superimposition of the helices in both of the six-helix bundles of the inward-facing conformation on the outward-facing model has an rmsd of 1.26 Å, suggesting that the two conformations are symmetrical. On the other hand, LacY is highly dynamic. Although ~75% of the side chains are hydrophobic and buried, ~85% of the backbone amide protons exchange with deuterium in 10–15 min at room temperature (20, 21), with 100% exchange at elevated, nondenaturing temperatures (22). Moreover, recent studies (18, 23) provide evidence for the involvement of an occluded conformer of LacY during turnover.

Unlike WT LacY, single-molecule FRET (24) and double electron-electron resonance (DEER) studies (18) with solubilized, purified C154G LacY, as well as site-directed alkylation (SDA) experiments with right-side-out membrane vesicles (25), show that galactoside binding leads to closing of the cytoplasmic cavity, although the periplasmic side remains paralyzed in an open conformation in presence or absence of sugar. Another relevant mutation regarding conformational dynamics is D68E or D68N, in which the periplasmic side is paralyzed in a closed conformation, whereas sugar binding causes closure of the cytoplasmic cavity (26). In addition, the C154G mutant (helix V), which exhibits little or no transport activity (27), is largely rescued by replacing Gly24, the neighboring residue in helix I, with Cys (28). Finally, cross-linking studies (29) demonstrate that restricting conformational flexibility between helices I and V within the N-terminal six-helix bundle impairs transport. The observations indicate that the structural dynamics of LacY during turnover likely involve more than rigid body movements (30).

A six-step kinetic scheme is useful for describing the general features of the alternating access model for active transport (Fig. 1*C*). In addition to inward- and outward-facing conformers (HE_i and HE_o), the scheme predicts that at least four other intermediates exist (E_i, E_o, HE_oS, and HE_iS). In this regard, for certain spin-labeled Cys pairs, three or four distance

Author contributions: M.G.M. and H.R.K. designed research; M.G.M. and S.N.S. performed research; M.G.M., S.N.S., and H.R.K. analyzed data; and M.G.M. and H.R.K. wrote the paper.

The authors declare no conflict of interest.

*This Direct Submission article had a prearranged editor.

[1]To whom correspondence should be addressed. E-mail: rkaback@mednet.ucla.edu.

See Author Summary on page 17740 (volume 109, number 44).

This article contains supporting information online at www.pnas.org/lookup/suppl/doi:10.1073/pnas.1211183109/-/DCSupplemental.

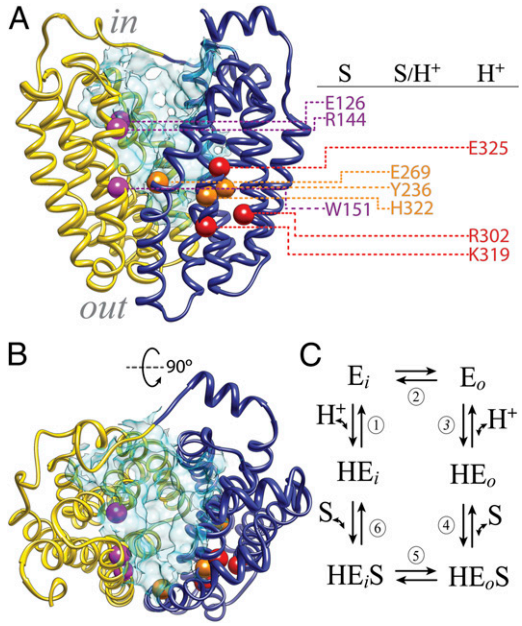

Fig. 1. LacY structure. (*A*) Side view of the inward-facing conformation of LacY (PDB ID code 2V8N). The N-terminal six-helix bundle is colored yellow, and the C-terminal six-helix bundle is colored dark blue. The cytoplasmic side (*in*) and the periplasmic side (*out*) are shown. The spheres represent Cα atoms of critical residues (magenta, residues involved in sugar binding exclusively; orange, residues involved in sugar affinity and H^+ translocation; red, residues involved in H^+ translocation exclusively; details are provided in the main text). The water-accessible surface of the cavity is shown in light blue (surface was calculated using the *Computed Atlas of Surface Topography of proteins* (CASTp) Web tool with a probe size of 1.4 Å). (*B*) Cytoplasmic view; the color coding is as in *A*. (*C*) Six-step kinetic model for lactose/H^+ symport. Steps are numbered consecutively: (1) deprotonation of inward-facing conformer (HE_i) resulting in the unprotonated inward-facing conformation (E_i), (2) conformational change allowing the galactoside- and H^+-binding sites to become accessible to the periplasmic side of the membrane (E_o), (3) protonation of LacY yielding the protonated and outward-facing conformer (HE_o), (4) substrate binding and formation of the sugar-bound protonated and outward-facing conformer (HE_oS), (5) global conformational change in which the protonated LacY with bound sugar returns to the initial inward-facing conformation (HE_iS), and (6) dissociation of sugar.

populations are resolved by DEER measurements, which supports the notion that additional conformers are present during turnover (18).

Recent studies with reconstituted LacY (31) provide kinetic evidence for a slow conformational transition preceding sugar binding from the periplasmic side. The turnover time of 16–20 s^{-1} estimated for uphill lactose/H^+ symport (i.e., active transport) (32) is virtually the same rate as observed for sugar binding to LacY in proteoliposomes (31). Therefore, opening of the periplasmic cavity is limiting for galactoside binding and may also be limiting for symport.

Using comparative modeling based on the X-ray crystal structures of LacY (11, 13, 14) and the oligopeptide/H^+ symporter (PepT) [Protein Data Bank (PDB) ID code 2XUT] (33), a structural model for an intermediate of LacY devoid of bound sugar (the apo-intermediate) is presented here. The model is consistent with numerous experimental data, particularly distance measurements obtained by DEER. Moreover, the results lead to two conclusions: (*i*) the model represents a feasible simulation of a LacY apo-intermediate, and (*ii*) a second occluded and protonated intermediate with bound sugar is present during turnover. An energy profile for the overall transport cycle is also presented.

Results

Apo-Intermediate of LacY. The model of the LacY apo-intermediate was built based on the crystal structure of PepT (PDB ID code 2XUT) (33). PepT contains 14 transmembrane helices, but helices HA and HB in the middle cytoplasmic loop are not conserved in the structures of other MFS transporters (11, 30, 34) (*SI Appendix*, Fig. S1). The primary constraints for comparative model building were obtained from structure-sequence alignments of LacY (13) with the EmrD (34), FucP (17), GlpT (30), and PepT (33) crystal structures, omitting helices HA and HB in PepT (*SI Appendix*, Fig. S1). The secondary structure of LacY observed in the crystal structure (11–14) was retained in the model-building procedure.

The model constructed displays a conformer with the sugar-binding site inaccessible for sugar from both sides of the membrane (Fig. 2). The overall architecture contains 12 transmembrane helices and the connecting loops. The model is composed of 374 residues (residues 7–194 and 214–401), with the great majority (94.4%) well within the allowed regions of the Ramachandran plot (*SI Appendix*, Fig. S3*A*). A discrete optimized protein energy (DOPE) profile was also calculated for all modeled and template structures. DOPE is an atomic distance-dependent statistical potential derived from a sample of native structures. Like the DOPE score itself, the profile is a theoretical energy measure of the finite and spherical shape of native structures (35). The DOPE profile for the model reveals a statistical potential profile similar to those calculated for the X-ray structures of WT LacY and PepT (*SI Appendix*, Fig. S3*B*), indicating similar statistical model qualities of the X-ray structures and the theoretical model.

The pseudosymmetry between the N- and C-terminal six-helix bundles observed in X-ray structures of MFS proteins (11–14, 17, 30, 34) is retained in the model of the outward-facing conformer of LacY (18, 19), as well as in the apo-intermediate model (rmsd of 3.5 Å compared with rmsd of 2.7 Å for the inward-facing conformation). However, unlike the case in the inward-facing conformation, where the six-helix bundles are related by a symmetry axis perpendicular to the membrane plane, the symmetry axis in the

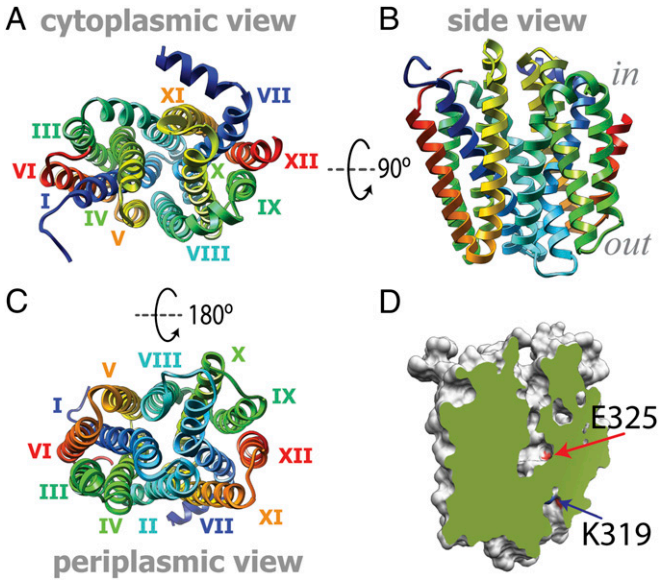

Fig. 2. Predicted tertiary structure model for the apo-intermediate. (*A*) Cytoplasmic view; the helices are numbered with roman numerals. (*B*) Side view; the color coding is as in *A*. (*C*) Periplasmic view; the color coding is as in *A*. (*D*) Slab view of the cavities in the apo-intermediate. The molecule surface is colored gray, and the exposed surface is colored green. The contact surfaces of residues K319 and E325, as indicated by the arrows (blue and red, respectively), are colored according to the heteroatom (red, oxygen; blue, nitrogen).

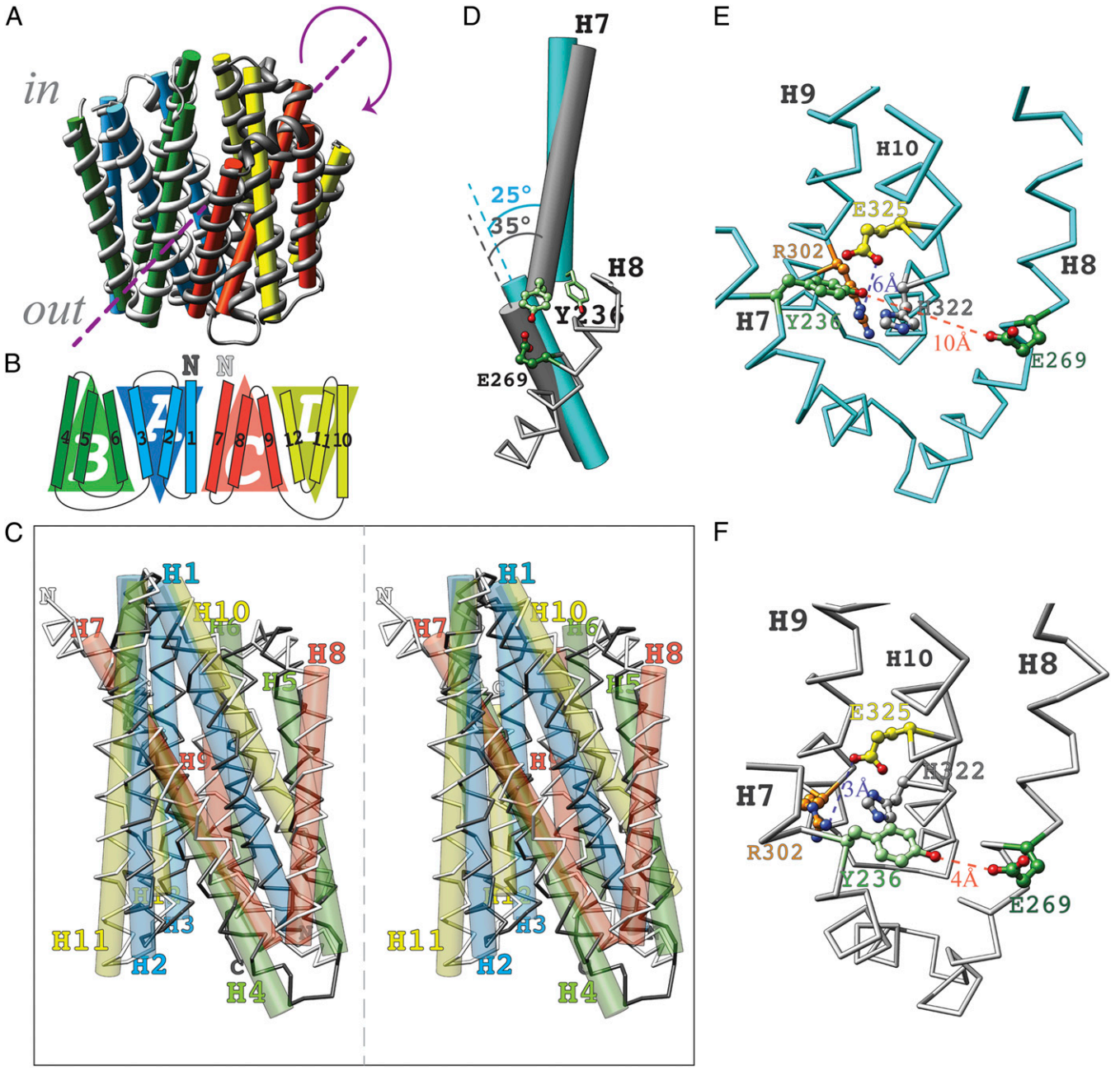

Fig. 3. Structural characteristics of the apo-intermediate. (*A*) Symmetry. The symmetry axis (broken line) is parallel to the membrane. (*B*) Schematic of the transmembrane topology of LacY emphasizes structural relationships between the four triple-helix topology segments. The N termini of the first (H1–H6) and second (H7–H12) six-helix bundles are indicated with a dark "N" and a light "N", respectively. (*C*) Structural alignment of the N-terminal and C-terminal six-helix bundles (stereoview). (*D*) Kink in helix 7. The helix-vectors of the N- and C-terminal parts of helix 7 are shown as rods, in cyan for the X-ray structure and in gray for the apo-intermediate model. Their crossing angels are indicated. Residue Y236 (pale green) is shown in two positions: as a stick model in the X-ray structure and as balls and sticks in the apo-intermediate model. For orientation, the chain trace of H8 in the apo-intermediate is shown in gray with the residue E269 (dark green). (*E*) Cytoplasmic view of the components of the H^+ translocation site according to the X-ray structure of the inward-facing conformation (PDB ID code 2V8N). The side chains are colored as follows: light green, Y236; dark green, E269; orange, R302; gray, H322; and yellow, E325. Oxygen and nitrogen atoms are colored red and blue, respectively. (*F*) Cytoplasmic view of the H^+ translocation site in the apo-intermediate model. Side chains are colored the same as in *E*.

model is parallel to the membrane (Fig. 3*A* and *SI Appendix*, Fig. S4). In this case, the first three-helix bundle (Fig. 3*B*; repeat-A, H1–H3) corresponds structurally to the fourth three-helix bundle (repeat-D, H10–H12), and the second three-helix bundle (repeat-B, H4–H6) corresponds structurally to the third three-helix bundle (repeat-C, H7–H9), resulting in a rotation of 180° with respect to the membrane (Fig. 3 *B* and *C* and *SI Appendix*, Fig. S4*B*, *ii* and *viii*). With the N termini of both six-helix bundles oriented to the same side of the membrane, the N-terminal six-helix bundle of the apo-intermediate can be superimposed on the N-terminal six-helix bundle of the outward-facing conformation. The C-terminal six-helix bundle of the apo-intermediate can be superimposed on the C-terminal six-helix bundle of the inward-facing conformation (*SI Appendix*, Fig. S5).

Comparison of the inward-facing X-ray structures with the apo-intermediate model suggests changes in the relative position of

residues in the H^+-binding site. Kinking of helix VII changes the crossing angle of the N- and C-terminal portions of this helix. In the inward-facing conformation, the N- and C-terminal parts cross at an angle of 25°, whereas in the apo-intermediate model, the crossing angle is 35° (Fig. 3*D*). This conformational transition moves Tyr236 into the vicinity of Glu269 (r = 4 Å) and allows the interaction of His322 with Glu325 (r = 3 Å; Fig. 3*F*). Moreover, the model also exhibits a narrow pathway leading from the periplasmic side to Arg302 and Lys319 close to the protonation site at the bottom of the major cavity (Fig. 2*D* and *SI Appendix*, Fig. S8).

Evaluation of the Model. The model was evaluated by comparing experimental distances obtained by DEER measurements of interhelical distances between nitroxide-labeled paired Cys replacements. Twenty-two nitroxide pairs were analyzed, 7 cytoplasmic and 15 periplasmic (20 on WT background and 2 on C154G mutant background; details are provided in Table 1). DEER measurements reveal two, three, or four distance populations for given pairs (18). The interhelical distances in the model were evaluated against experimentally measured distances (Table 1 and *SI Appendix*, Table S1). Nitroxides were modeled at positions of the Cys replacements. After optimization for clashes with the protein, the dihedral angles of labeled triplets were varied (3 at a time) to find conformations of the nitroxide radicals that satisfy the interspin distances from the DEER measurements (Fig. 4 and *SI Appendix*, Table S2) and the conformational restraints for the nitroxide labels (36).

Analysis of WT LacY and Mutants. X-ray structures of LacY in the inward-facing conformation (11–14), the predicted structure of the outward-facing conformation (19), and the model of the apo-intermediate allow assignment of interspin distances (18) corresponding to individual conformational states estimated from the interspin distances (Figs. 5 and 6). For the cytoplasmic pairs, the longest interspin distances are attributed to the inward-facing conformation of LacY, with an open cytoplasmic cavity and the shortest distances attributed to the outward-facing conformation with a closed cytoplasmic cavity (18). All Cys pairs (Table 1) were analyzed in the same fashion; an example for two pairs, one periplasmic and one cytoplasmic, is presented in Figs. 5 and 6. The cytoplasmic nitroxide pair 73/340 reveals multiple interspin distances, indicating multiple conformations of LacY in the steady state (Fig. 5). In the absence of bound sugar (NPGlu, 4-nitrophenyl-α-D-glucopyranoside), the distance between peak centers of the longest and shortest interspin distances of nitroxide

Table 1. Comparison of experimental interspin distances attributed to the apo-intermediate (DEER) with distances between the respective modeled nitroxide pairs (Model)

Pair	DEER, Å	Model, Å	Pair	DEER, Å	Model, Å
36/310*	31–33	29	73/401†	37–38	39
41/164*	28	26	105/249*	27	29
41/252*	28	26	105/310†	39–40	39
41/255*	31–33	29	136/401†	37	35
41/310*	30	28	137/340†	32–33	31
43/164*	27	28	137/401†	31	34
43/252*	29	29	164/310†	31 (31)	31
43/255*	32	30	164/371*	32	35
43/310*	30	30	164/372*	25	25
73/340†	34 (35)	35	164/375†	34	35

Interspin distances in parentheses were measured on the background of the C154G mutant.

*Relative distributions of conformational populations calculated from multi-Gaussian fits presented in *SI Appendix*, Table S1.

†Relative distributions of conformational populations calculated from multi-Gaussian fits taken from the study by Smirnova et al. (18).

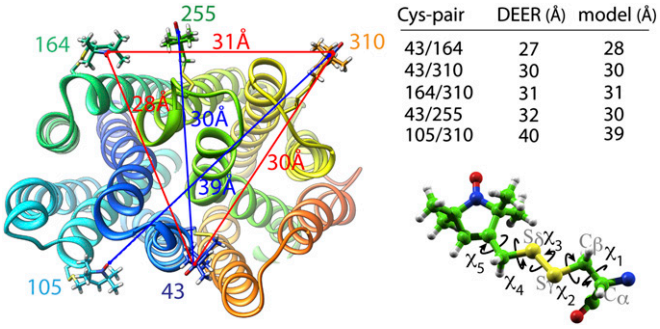

Fig. 4. Distance trilateration. Nitroxide labels attached to paired Cys replacements are modeled on the proposed apo-intermediate and optimized for clashes with the protein surface (*Left*). Conformational space was explored by varying the χ-angle (*Lower Right*) to find conformations of nitroxide side chains that satisfy DEER distances between three residues (*Upper Right*) [i.e., residues 43–164, 164–310, and 43–310, indicated with red lines (*Left*)] as described in *Experimental Procedures*. The next residue (i.e., residue 255) was modeled, and the next trilateration set is optimized in agreement with the DEER data. The distances are taken from a study by Smirnova et al. (18) and *SI Appendix*, Table S2.

pairs at positions 73 and 340 is 21 Å (Fig. 5*A*; 44 Å, green; 23 Å, blue). This difference agrees well with the 17.2-Å difference between the Cα atoms at positions 73 and 340 in the X-ray structure (13) and the postulated outward-facing conformer (19). The distance between nitroxides at positions 73 and 340 in the model for the apo-intermediate (Table 1, 35 Å) corresponds to the intermediate interspin distance of 34 Å in the presence of bound 4-nitrophenyl-α-D-galactopyranoside (NPGal) (Fig. 5*B*, orange). The distance difference between the respective peak centers in the DEER experiment (Fig. 5*B*, 10 Å) is in good agreement with the distance difference between the respective Cα atoms in the models of the inward-facing crystal structure and the apo-intermediate (6.5 Å). The distance difference between the peak center attributed to the outward-facing conformation (Fig. 5*A*, 23 Å, blue) and the peak center attributed to the apo-intermediate (Fig. 5*B*, 34 Å, orange) is also in agreement with the distance difference between Cα atoms in the outward-facing and apo-intermediate models (10.7 Å).

Similarly, interspin distances on the periplasmic side are attributed to respective conformers (Fig. 6 *A* and *B*). Cα atoms of Cys pair 164/310 exhibit a distance difference of 10.3 Å between the inward-facing X-ray structure (13) and the model of the outward-facing conformation (19). This agrees with the difference between the peak centers of interspin distances at 35 Å and 45 Å, respectively (Fig. 6*A*), attributed to the inward-facing (Fig. 6*A*, green) and outward-facing (Fig. 6*A*, blue) conformations on the periplasmic side. Modeling the nitroxides at positions 164 and 310 allows assignment of the peak center at 31 Å (Fig. 6*A*) to the apo-intermediate (Fig. 6*A*, orange). The distance difference between the Cα atoms in the crystal structure of the inward-facing conformation and the model of the apo-intermediate reveals longer distances, which agrees with the DEER measurements. Galactoside binding triggers opening of the periplasmic cavity, and consequently results in an increase in the long interspin distance population (Fig. 6, blue) on the periplasmic side. The apo-intermediate population (Fig. 6*B*, orange) is attenuated on NPGal binding, and a shorter distance population appears (Fig. 6*B*, gray).

To examine whether the occurrence of the modeled intermediate is sugar-dependent, the median interspin distances (Figs. 5 and 6, gray and orange) for pairs 73/340, 136/340, 137/340, and 137/401 on the cytoplasmic side and for pairs 164/310, 105/310, 164/372, and 41/255 on the periplasmic side were analyzed for changes of fractional distributions on binding of galactoside

(Fig. 7). A strong correlation is observed between galactoside binding and the occurrence of a median interspin distance that is

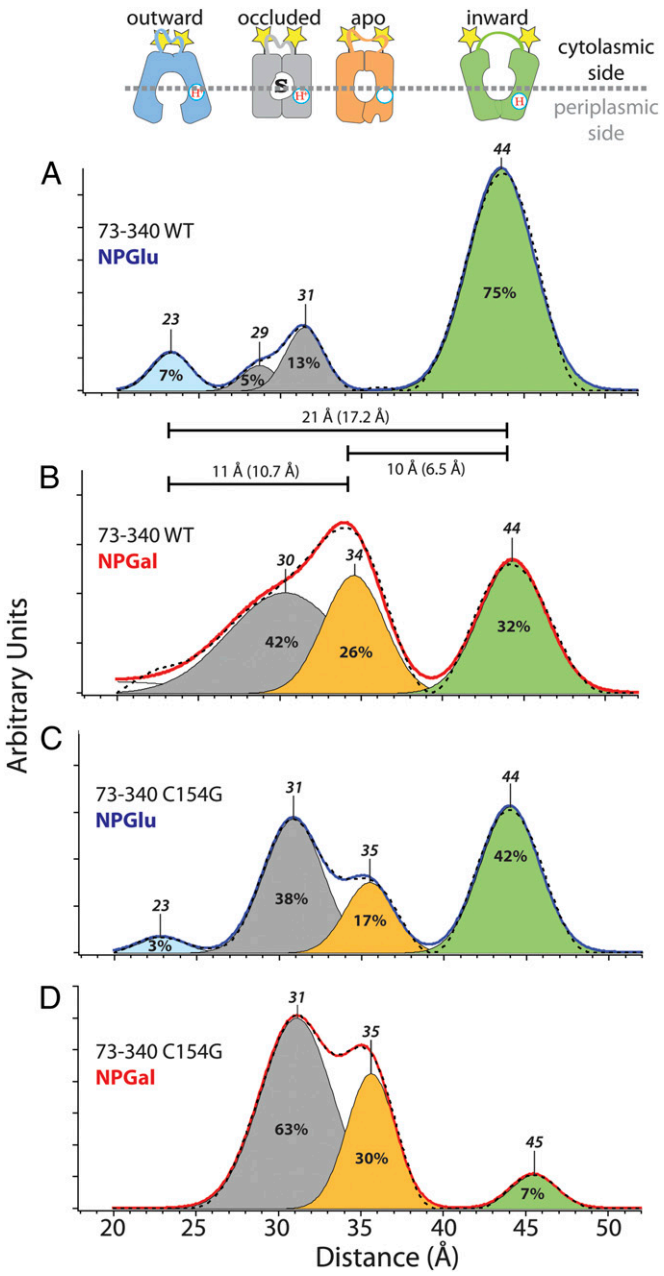

Fig. 5. Interspin distance distributions detected with nitroxide-labeled cytoplasmic Cys pair 73/340 (indicated by yellow stars) on WT LacY (*A* and *B*) or mutant C154G (*C* and *D*). Distance distributions obtained by Tikhonov regularization of dipolar spectra are shown (*A* and *C*, solid blue line with no bound sugar; *B* and *D*, solid red line with bound sugar). Relative distributions of conformational populations are obtained by multi-Gaussian deconvolution [details are provided in the study by Smirnova et al. (18)]. Peak centers, indicated on top of the Gaussian peaks, represent the distance between the nitroxides at these positions (interspin distance). The interspin distances are attributed to a distinct conformation (shown on top: blue, outward-facing; gray, occluded-intermediate; orange, apo-intermediate; green, inward-facing). The relative area of the respective Gaussian peaks is indicated (%) and represents the fraction of each conformational population in the multi-Gaussian fit (broken black line). The distance differences between the peak centers represent distance changes between these positions in different conformations and are indicated as horizontal bars. The numbers in parentheses are the distance differences between Cα atoms in the structure models of the respective conformations.

covered by the postulated occluded-intermediate (Fig. 7*A*). In contrast, the interspin distance populations on the periplasmic side covered by the apo-intermediate exhibit a decrease in the presence of ligand (Fig. 7*B*). On the cytoplasmic side, the distance fractions attributed to the apo-intermediate are very small, and they increase on sugar binding. However, the increase observed on sugar binding is always lower (Fig. 7*B*, cytoplasmic side) than the increase in conformational fractions attributed to the protonated, sugar-bound occluded-intermediate (Fig. 7*A*, cytoplasmic side).

Comparison of the interspin distances measured with cytoplasmic nitroxide pairs in mutant C154G reveals interspin distances that overlap with distances obtained with WT LacY (Fig. 5 *C* and *D*). WT LacY responds to sugar binding with a shift primarily from an inward-facing conformer with a long interspin distance (Fig. 5*A*, 44 Å, green) to a distance commensurate with the occluded-intermediate (Fig. 5*B*, 30 Å, gray) and the apo-intermediate (Fig. 5*B*, 34 Å, orange). In contrast, mutant C154G in the absence of ligand (Fig. 5*C*) exhibits a disperse conformational population similar to that of the WT in the presence of NPGal (Fig. 5*B*). Addition of sugar to mutant C154G increases the occurrence of the occluded-intermediate (Fig. 5*D*, gray) and the apo-intermediate (Fig. 5*D*, orange), and the interspin distance population of the inward-facing conformation (Fig. 5*D*, green) is severely attenuated. The major conformational fraction on the periplasmic side of the mutant is the outward-open conformation (Fig. 6*C*, blue). Sugar binding enhances the conformational fractions of the apo-intermediate (Fig. 6*D*, orange) and the inward-facing conformation (Fig. 6*D*, green). However, the interspin distance assigned to the open periplasmic cavity (Fig. 6*D*, 45 Å, blue) accounts for the major portion of the populations.

Discussion

Structure. The hallmark of the MFS is diversity. Although it is likely that the members all function by alternating access of binding sites to either side of the membrane and they share a common protein fold, very different substrates are transported by uniport, symport, or antiport mechanisms (1, 2). Therefore, the proteins in the superfamily do not share extended sequence homology because substrate and cosubstrate binding sites, as well as modes of transport, are different. However, comparison of the available structure data for members of the superfamily reveals uniformity of the individual helices with respect to kinks and bends. At these positions, sequence comparisons exhibit residues that promote irregularities in helices (i.e., Pro, Lys, Asp, Ser, Thr, Cys, Gly) (37). A sequence alignment of LacY, PepT (33), and EmrD (34) based on helix irregularities was used to calculate the apo-intermediate model of LacY (*SI Appendix*, Fig. S2 and *SI Text*).

The resulting model displays a central twofold pseudosymmetry between both of the six-helix bundles. Symmetry between the N- and C-terminal bundles has been documented in the X-ray structures of MFS proteins (11–14, 30, 34) and in the model of the outward-facing LacY conformer (19). However, unlike the inward- or outward-facing conformers, which are structurally related by a symmetry axis perpendicular to the membrane (*SI Appendix*, Fig. S4 *A* and *C*), in the model for the LacY apo-intermediate, the symmetry axis is parallel to the membrane (Fig. 3 *A*–*C*). This results in a structural alignment with a single six-helix bundle rotated by 180° with respect to the membrane (Fig. 3*C*). The inverted topology repeats exhibit swapped conformations in the outward-facing model of LacY, as suggested by Radestock and Forrest (19), compared with the inward-facing conformation (*SI Appendix*, Fig. S4 *A*, *i* and *C*, *iii*). However, in the apo-intermediate, only a single six-helix bundle shows swapped conformations of inverted repeats A and B (Fig. 3*B*). This observation argues against a rocker-switch model according to which the conformational changes are believed to be symmetrical (11, 30, 38).

The predicted apo-intermediate model was tested for the presence of observed interspin distances. However, not all nitroxide

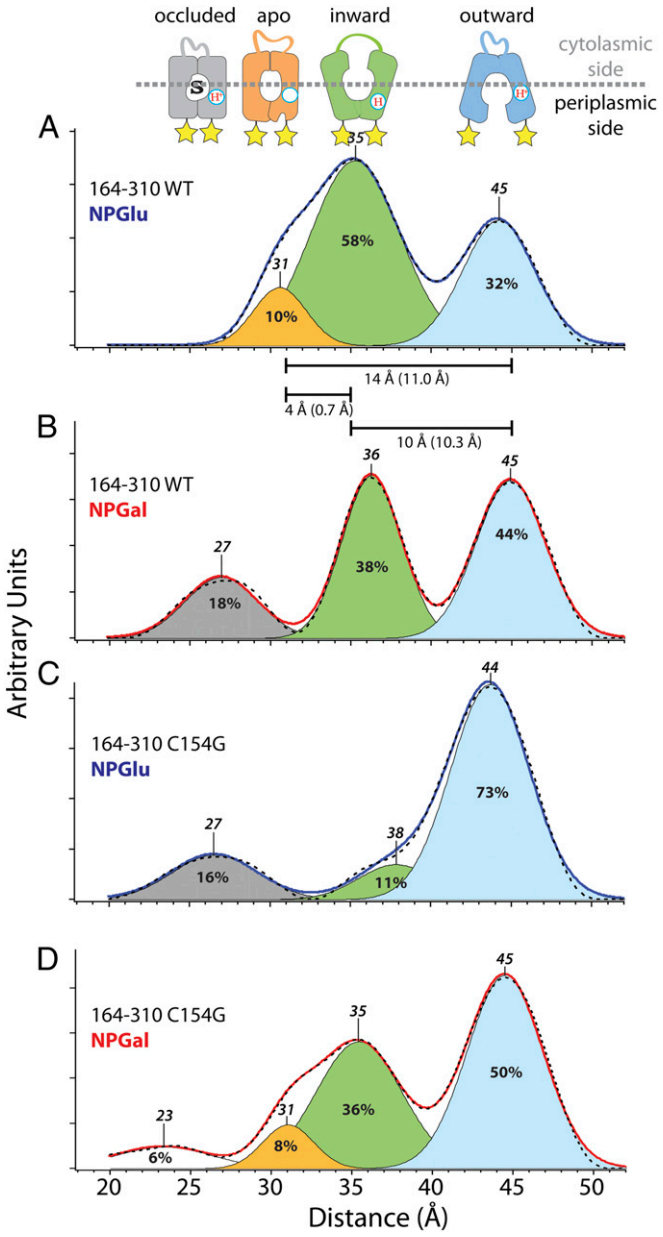

Fig. 6. Interspin distance distributions detected with nitroxide-labeled periplasmic Cys pair 164/310 (indicated by yellow stars) on WT LacY (*A* and *B*) or mutant C154G (C and *D*). Distance distributions obtained by Tikhonov regularization of dipolar spectra are shown (*A* and *C*, solid blue line with no bound sugar; *B* and *D*, solid red line with bound sugar). Relative distributions of conformational populations are obtained by multi-Gaussian deconvolution [details are provided in the study by Smirnova et al. (18)]. Peak centers, indicated on top of the Gaussian peaks, represent the distance between the nitroxides at these positions (interspin distance). The interspin distances are attributed to a distinct conformation (shown above: blue, outward-facing; gray, occluded-intermediate; orange, apo-intermediate; green, inward-facing; white, unassigned). The relative area of the respective Gaussian peaks is indicated (%) and represents the fraction of each conformational population in the multi-Gaussian fit (dashed black line). The distance differences between the peak centers represent distance changes between these positions in different conformations and are indicated as horizontal bars. The numbers in parentheses are the distance differences between Cα atoms in the structure models of the respective conformation.

pairs exhibit four distance populations, mainly because interspin distances between nitroxide pairs may overlap in different conformers. Nevertheless, the shortest and longest distances were attributed to the open conformer (longest distance) and closed conformer (shortest distance) on the respective sides of LacY, and the intermediate distances were attributed to the protonated sugar-bound conformer (18). However, the occurrence of two intermediate distances suggests the presence of two structurally distinct intermediate conformations. Analysis of intermediate interspin distances reveals a significant difference. Galactoside binding facilitates the occurrence of conformers with intermediate distances that are not observed in the apo-intermediate model on either side of LacY (Fig. 7*A*). Therefore, the interspin distances whose occurrence is enhanced by galactoside binding are assigned to the protonated occluded-intermediate conformations, which bind sugar. The distances observed in the apo-intermediate do not depend on binding of sugar; therefore, the model likely represents the sugar-free apo-intermediate (Fig. 7*B*).

The distances between Cα atoms on the periplasmic side across the central cavity reveal tighter packing of the helices in the apo-intermediate relative to the inward-facing conformation (Table 2). Thus, distances attributed to the apo-intermediate are shorter compared with those attributed to the inward-facing conformation (Fig. 6*A* and Table 2). Correlated with the decreased distance is the appearance of a minor cavity between helices VII, IX, and XII on the periplasmic side leading to Arg302 and Lys319

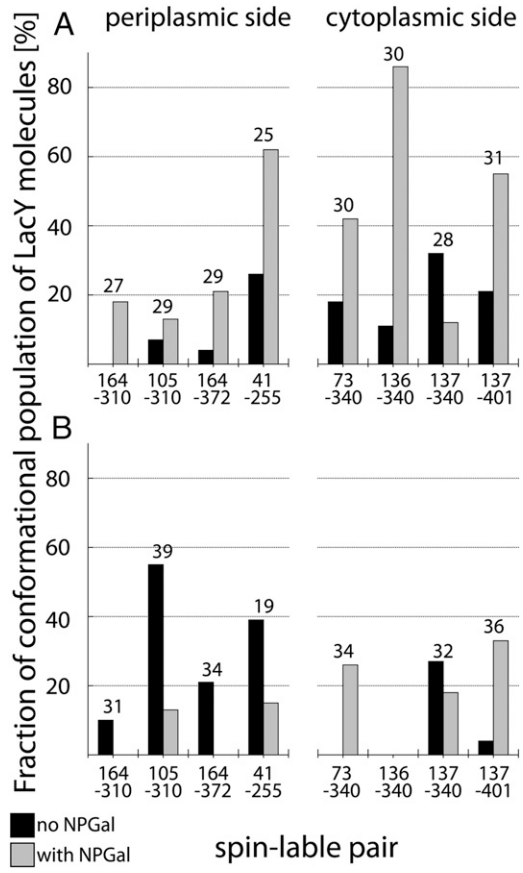

Fig. 7. Effect of sugar binding on fraction distribution of apo-intermediate and occluded-intermediate. Vertical bars represent the relative fraction of conformational population calculated from multi-Gaussian deconvolution of distributions obtained by Tikhonov regularization [details are provided in the study by Smirnova et al. (18)]. Results attributed to the occluded-intermediate (*A*) and apo-intermediate (*B*) with no sugar bound (black bars) or in the presence of a saturating concentration of NPGal (gray bars) are compared. Periplasmic Cys pairs (*Left*) and cytoplasmic Cys pairs (*Right*) are shown. The peak center distances (expressed in angstroms) assigned to the respective conformations are indicated above the data pairs.

Table 2. Comparison of measured interspin distance changes with predicted distance changes between Cα atoms in LacY structure models (model)

	73–340		43–252		43–255		164–310	
Pair	Apo	Out	Apo	Out	Apo	Out	Apo	Out
In (model)	−6.5	−17.2	−8.4	+6.6	−7.9	+8.5	+0.7	+10.3
In (DEER)	−10	−21	−11	+7	−7	+7	+4	+10
Apo (model)		−10.7		+15		+16.4		+14
Apo (DEER)		−11		+12		+13		+11

Conformations with accessible structure models are compared. Apo, apo-intermediate; In, inward-facing; Out, outward-facing.

(Fig. 2*D* and *SI Appendix*, Fig. S8), which are involved in H^+ translocation (7, 10, 39, 40). This highlights the minor cavity as an attractive point for H^+ access from the periplasmic side.

Interspin Distance Correlations. In WT LacY, the cytoplasmic and periplasmic cavities open and close in reciprocal fashion. However, it has also been shown that in certain mutants, the cavities can operate in an uncoordinated manner (23, 25, 26, 29). Comparison of conformational fractions on opposite sides of LacY reveals asymmetrical conformations (Fig. 7). This is most clearly demonstrated by the example of nitroxide pairs 73/340 and 164/310 (Figs. 5 and 6). Interspin distances corresponding to the occluded-intermediate on the cytoplasmic side occur in the absence of sugar (Fig. 5*A*, gray); however, the corresponding distances of an occluded-intermediate are not observed on the periplasmic side (Fig. 6*A*). On the contrary, interspin distances that match the apo-intermediate detected on the periplasmic side (Fig. 6*A*, orange) are absent on the cytoplasmic side (Fig. 5*A*). Furthermore, binding of sugar induces conformational changes on the cytoplasmic side that are consistent with the occluded-intermediate (correlation with the EM density map of OxlT is discussed in *SI Appendix*, *SI Text*, Fig. S6). Thus, the occurrence of mixed conformational states with closed and open cavities on the opposite sides of the molecule is a clear possibility so long as both cavities are not open simultaneously.

Conformer Fractions. Interspin distance measurements with WT LacY reveal a conformational distribution bias toward an inward-facing conformation (Fig. 5*A*, green). In the absence of sugar, the sum of the cytoplasmic conformer fractions attributed to the outward-facing (Fig. 5*A*, blue) and occluded (Fig. 5*A*, gray) conformations [Fig. 5*A*, 23 Å, 29 Å, and 31 Å (25% of total)] agrees roughly with the fraction of the outward-facing conformer population on the periplasmic side [Fig. 6*A*, 45 Å (32% of total, blue)]. The longest distance fraction on the cytoplasmic side [Fig. 5*A*, 44 Å (75% of total, green)] is approximately the sum of the inward-facing fraction [Fig. 6*A*, 35 Å (58% of total, green)] and the apo-intermediate fraction [Fig. 6*A*, 31 Å (10% of total, orange)] on the periplasmic side. Therefore, all conformations are accounted for except the fully closed occluded- and apo-intermediates. Apparently, the inward-open conformer represents a mixture of different conformational states. When a galactoside is bound, a significant increase in the occurrence of conformers populating interspin distances corresponding to the occluded state (Figs. 5*B* and 6*B*, gray; 30 Å and 27 Å, respectively) is observed. As a result, the fractions of the inward-facing conformers are equal on both sides [Figs. 5*B*, 44 Å (32% of total, green) and 6*B*, 36 Å (38% of total, green)] and approximate the fraction of the outward-facing conformers [Fig. 6*B*, 45 Å (44% of total, blue)], suggesting relatively similar free energy levels and an unhindered transition between the conformers. Thus, LacY operates in a very similar fashion to an enzyme, except that the intermediate is a conformer(s) of the symporter rather than a transition state intermediate of the substrate (41). In this view, the intermediate conformation is induced by sugar binding and leads to lowering of the activation energy barrier for the transition between the inward-facing and outward-facing conformers.

The conformationally restricted mutant C154G exhibits unique properties compared with WT LacY. Although transport is almost negligible, the mutant binds galactosides as well as or even better than the WT and is not leaky to H^+ (27, 42–44), thereby suggesting that the C154G mutant likely assumes an intermediate conformation on sugar binding (23, 43). The fractional distribution of cytoplasmic distances observed with the C154G mutant in the absence of sugar is similar to that of WT LacY in presence of sugar (Fig. 5 *B* and *C*), and the periplasmic interspin distances

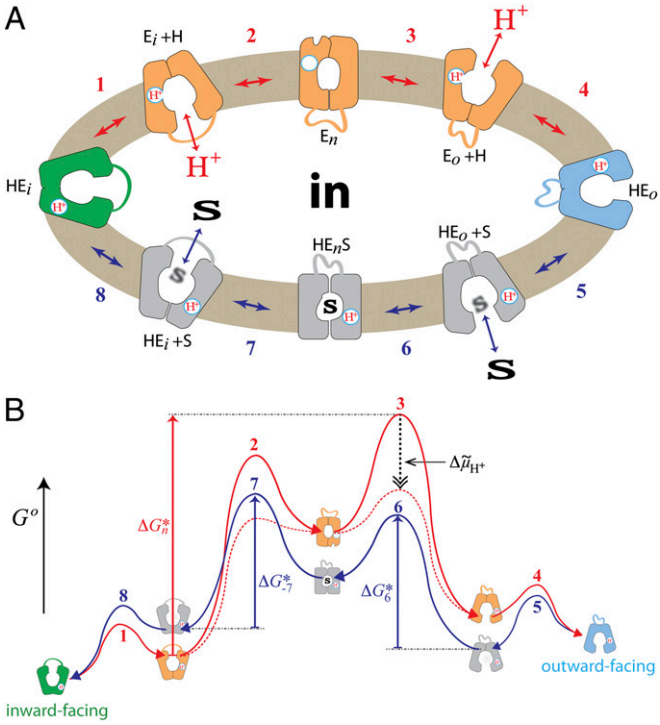

Fig. 8. Transport cycle of LacY. (*A*) Overview of the postulated steps in the transport model. Inward-facing (green) and outward-facing (blue) conformations are separated by the apo-intermediate conformational cluster (orange) or by the occluded-intermediate conformational cluster (gray). Steps are numbered consecutively: (1) conformational transition allowing the deprotonation of Glu325; (2) formation of the deprotonated apo-intermediate; (3) reprotonation of LacY and opening of the periplasmic cavity; (4 and 5) reorientation of helices, where LacY passes through a low-energy conformation (details are provided in the main text); (6) binding of sugar and induced fit to the occluded-intermediate; (7) opening of the cytoplasmic cavity and release of sugar; and (8) conformational transition to inward-facing conformation. All steps are reversible (indicated by double-headed arrows). (*B*) Hypothetical energy profile for the transport cycle. Conformational states in *A* are translated into relative energy states (indicated by the icons of conformations defined in *A* with the cytoplasmic side of LacY facing up) based on their occurrence as a conformational fraction in interspin distance distribution. The scheme can be read in cycle following the arrowheads. The red line represents the transition between steps 1 and 4 for opening of the empty carrier to the outward-facing conformation. The blue line corresponds to steps 5–8 for sugar transport from outside to inside (and to the exchange reaction when steps 5–8 operate in a reverse manner). The free energy of the putative rate-determining step in absence of $\Delta\tilde{\mu}_H{}^+$ (opening of the periplasmic cavity) is indicated by the vertical red arrow ($\Delta G_n{}^*$). The hypothetical effect of an imposed $\Delta\tilde{\mu}_H{}^+$ is shown as a dashed black vertical arrow, and the resulting energy profile is shown by the dashed red lines. The energy of sugar binding on the periplasmic (ΔG^*_6) and cytoplasmic (ΔG^*_{-7}) sides is suggested to be equivalent from either side of the membrane (indicated by the vertical blue arrows).

indicate an open periplasmic cavity (Fig. 6*C*, blue). Therefore, the mixture of conformers observed in the mutant is similar to that observed with WT LacY in the presence of NPGal. When the mutant binds sugar, the interspin distances on the cytoplasmic side populate predominantly intermediate distances (Fig. 5*D*, gray and orange) and the long-distance fraction (Fig. 5 *C* and *D*, 44/45 Å, green) is drastically decreased. Thus, unlike WT LacY, where the opening probability of the cytoplasmic cavity decreases somewhat in the presence of galactoside, the opening probability of the cytoplasmic cavity in the C154G mutant decreases dramatically in the presence of sugar. In the C154G mutant with bound sugar, interspin distances of the periplasmic nitroxide pair assume a similar distribution to WT LacY without bound sugar (Fig. 6 *A* and *D*), but an increased contribution of the open periplasmic cavity (Fig. 6 *A* and *D*, blue) is observed. The conclusions are consistent with SDA results (23) showing that Cys replacements on the periplasmic side of the sugar-binding site in C154G LacY are highly reactive/accessible in the absence of sugar. However, on the cytoplasmic side, labeling of the single-Cys mutants decreases on sugar binding, as observed with WT LacY.

Energy Profile of Transport. Based on these results, an energy profile of the overall transport cycle is postulated (Fig. 8). The sequence is initiated from the inward-facing conformer (HE_i) in which Glu325 is protonated due to the low dielectric of the local environment of the carboxylate. Deprotonation of Glu325 is caused by the proximity of Arg302 (10, 40) (step 1); subsequently, the cytoplasmic cavity closes (step 2), resulting in the formation of the high-energy apo-intermediate (E_n). E_n can relax back to the inward-facing conformation or open and become protonated on the periplasmic side (step 3). To bind sugar on the periplasmic side, reorientation of helices is necessary (e.g., rotation of helices IV and X as discussed in *SI Appendix*, *SI Text*), and the protein passes through a low-energy conformer symmetrical to the inward-facing form (HE_o, steps 4 and 5). Binding of sugar induces the formation of the high-energy occluded state (HE_nS, step 6). This conformer can either relax to the outward-facing form or open the cytoplasmic cavity with release of sugar to the cytoplasm (step 7) and reorientation of the helices. Protonated LacY then passes through a low-energy conformer (HE_i) to a conformer that releases H^+, and the cycle is reinitiated (steps 8 and 1).

Semiquantitative survey of fractional distribution among individual distance populations attributed to distinct conformations allows a rough estimation of the relative occurrence of conformers at equilibrium and, consequently, relative energy states (Fig. 8*B*). In the postulated energy profile, the transport reaction (Fig. 8*A*) is presented as a cycle numbered inward- to outward-facing following the red lines (Fig. 8 *A* and *B*, opening of empty LacY to the periplasm, steps 1–4) and from outward-facing to inward-facing following the blue lines (Fig. 8 *A* and *B*, transport of sugar from periplasm to cytoplasm, steps 5–8). High occurrence signifies a low-energy state [Fig. 8 *A* and *B* (i.e., HE_i, green)], and low occurrence signifies a high-energy state [Fig. 8 *A* and *B* (i.e., E_o + H, orange)]. The inward-facing (HE_i + S, HE_i, and E_i + H) and outward-facing (E_o + H, HE_o, and HE_o + S) conformations have relatively similar energy levels, but they are separated by the high-energy intermediates (Fig. 8 *A* and *B*; HE_nS, gray; E_n, orange). Substrate stabilizes the symmetrical occluded-intermediate (Fig. 8 *A* and *B*, HE_nS, gray), lowering the activation energy barrier between the outward-facing and inward-facing conformations (steps 6 and 7). Upon sugar binding, LacY exists largely in the occluded-intermediate state (Fig. 8*A*, HE_nS, gray), and due to its high-energy level, the frequency of relaxation to an outward-facing conformation is higher than for an inward-facing conformation. Consequently, the rate of opening to the periplasmic side is significantly increased.

Under exchange conditions (Fig. 8 *A* and *B*, dark blue, steps 5–8), transport proceeds at the same rate in both directions. Therefore, the activation energy barriers must be equal from both sides (Fig. 8*B*, blue arrows, $\Delta G^*_6 = \Delta G^*_{-7}$). Such energetic disposition, where high-energy barriers separate the inward- and outward-facing conformers, indicates the transport reaction to be kinetically controlled. Accordingly, if a sugar gradient drives the reaction, the rate-limiting step is the opening of the periplasmic cavity (31) (Fig. 8*B*, steps 2 and 3, ΔG_n^*). In presence of a $\Delta\tilde{\mu}_H{}^+$ (inside negative and/or alkaline; Fig. 8*B*, broken black arrow), where the deprotonation (step 2) and the reprotonation from the periplasm (step 3) are favored, the activation energy barriers of these steps are lowered (Fig. 8*B*, broken red line) and dissociation of sugar or conformational change becomes rate-limiting. Because $\Delta\tilde{\mu}_H{}^+$ does not influence exchange (45), the activation energy barriers for sugar binding (Fig. 8*B*, dark blue) from both sides must be lower than the activation energy barriers for opening empty LacY.

Although the relative energy barriers for the formation of the occluded- and apo-intermediates are equal from each side of the membrane (Fig. 8*B*, $\Delta G^*_6 = \Delta G^*_{-7}$) due to the different energy levels of the outward-facing and inward-facing conformations, the effect of galactoside binding or $\Delta\tilde{\mu}_H{}^+$ is different. Whereas saturating sugar concentrations would increase the occurrence of the open periplasmic cavity, an imposed $\Delta\tilde{\mu}_H{}^+$ would not have an effect on the conformational dispersion of LacY but only on the transition rates.

Experimental Procedures

Comparative Modeling of the LacY Apo-Intermediate. Comparative modeling was performed using the default-modeling schedule of MODELLER (version 9.8) with "Thorough Variable Target Function Schedule" and "Slow MD Annealing" (46). The X-ray structure of the oligopeptide/H^+ symporter, $PepT_{So}$ (PDB ID code 2XUT) (33) was used as a template, omitting transmembrane helices A and B, which are not present in LacY. The initial sequence alignment was generated by superposition of the LacY helix triplets on PepT and then improved manually by removing gaps within the helices. The target sequence was divided into 46 α-helical segments based on analysis of H-bonds in the transmembrane helices of LacY. The segments were kept constant as α-helical motifs throughout the modeling process. The central loop (195–213) was omitted from the modeling procedure.

Modeling of spin-labeled mutants is based on the proposed structure of the apo-intermediate of LacY. Native amino acids at the positions indicated were replaced by Cys residues, which were then reacted with nitroxide spin label (18). Nitroxide side chains in α-helices were set to adopt one of three rotamers with respect to the χ_1- and χ_2-dihedral angles [Fig. 4 and *SI Appendix*, Table S2; nominally, $m = -60°$, $P = +60°$, and $t = 180°$ ($\pm 30°$)] (36, 47). The dihedral angle χ_3 between Sγ and Sδ was restrained to only two conformations at +90° and −90°, and the side chain was optimizing for clashes and H-bonds with the protein. Trilateration of three measured distances was used to analyze the model.

Docking of LacY Apo-Intermediate Model into OxlT EM Density Map. The orientation of the apo-intermediate model of LacY in the density map of OxlT (48) was determined from the best correlation value of the simulated map of LacY at 6.5 Å. Docking of the model to the density map was performed using the program Chimera (49). Segmentation of the OxlT density map was performed using watershed segmentation (50). Watershed regions were grouped according to their connection at indicated density levels and correspondence to a given helix. The process was controlled interactively.

ACKNOWLEDGMENTS. We thank Irina Smirnova, Vladimir Kasho, Christian Altenbach, and Wayne L. Hubbell for providing the unpublished DEER data used in this work, and we particularly thank Irina Smirnova for her magnanimous help with the manuscript. This work was supported by National Institutes of Health Grants DK51131, DK069463, and GM074929, as well as by National Science Foundation Grant 0450970 (all to H.R.K.).

1. Saier MH, Jr. (2000) Families of transmembrane sugar transport proteins. *Mol Microbiol* 35:699–710.
2. Saier MH, Jr., et al. (1999) The major facilitator superfamily. *J Mol Microbiol Biotechnol* 1:257–279.
3. West IC (1970) Lactose transport coupled to proton movements in *Escherichia coli*. *Biochem Biophys Res Commun* 41:655–661.
4. West IC, Mitchell P (1973) Stoicheiometry of lactose-H+ symport across the plasma membrane of Escherichia coli. *Biochem J* 132:587–592.

5. Patel L, Garcia ML, Kaback HR (1982) Direct measurement of lactose/proton symport in Escherichia coli membrane vesicles: Further evidence for the involvement of histidine residue(s). *Biochemistry* 21:5805–5810.
6. Garcia-Celma JJ, Smirnova IN, Kaback HR, Fendler K (2009) Electrophysiological characterization of LacY. *Proc Natl Acad Sci USA* 106:7373–7378.
7. Guan L, Kaback HR (2006) Lessons from lactose permease. *Annu Rev Biophys Biomol Struct* 35:67–91.
8. Smirnova I, Kasho V, Kaback HR (2011) Lactose permease and the alternating access mechanism. *Biochemistry* 50:9684–9693.
9. Frillingos S, Sahin-Tóth M, Wu J, Kaback HR (1998) Cys-scanning mutagenesis: A novel approach to structure function relationships in polytopic membrane proteins. *FASEB J* 12:1281–1299.
10. Smirnova IN, Kasho VN, Sugihara J, Choe JY, Kaback HR (2009) Residues in the H+ translocation site define the pKa for sugar binding to LacY. *Biochemistry* 48: 8852–8860.
11. Abramson J, et al. (2003) Structure and mechanism of the lactose permease of Escherichia coli. *Science* 301:610–615.
12. Chaptal V, et al. (2011) Crystal structure of lactose permease in complex with an affinity inactivator yields unique insight into sugar recognition. *Proc Natl Acad Sci USA* 108:9361–9366.
13. Guan L, Mirza O, Verner G, Iwata S, Kaback HR (2007) Structural determination of wild-type lactose permease. *Proc Natl Acad Sci USA* 104:15294–15298.
14. Mirza O, Guan L, Verner G, Iwata S, Kaback HR (2006) Structural evidence for induced fit and a mechanism for sugar/H+ symport in LacY. *EMBO J* 25:1177–1183.
15. Kaback HR, Sahin-Tóth M, Weinglass AB (2001) The kamikaze approach to membrane transport. *Nat Rev Mol Cell Biol* 2:610–620.
16. Kaczorowski GJ, Kaback HR (1979) Mechanism of lactose translocation in membrane vesicles from *Escherichia coli*. 1. Effect of pH on efflux, exchange, and counterflow. *Biochemistry* 18:3691–3697.
17. Dang S, et al. (2010) Structure of a fucose transporter in an outward-open conformation. *Nature* 467:734–738.
18. Smirnova I, et al. (2007) Sugar binding induces an outward facing conformation of LacY. *Proc Natl Acad Sci USA* 104:16504–16509.
19. Radestock S, Forrest LR (2011) The alternating-access mechanism of MFS transporters arises from inverted-topology repeats. *J Mol Biol* 407:698–715.
20. le Coutre J, Kaback HR, Patel CK, Heginbotham L, Miller C (1998) Fourier transform infrared spectroscopy reveals a rigid alpha-helical assembly for the tetrameric Streptomyces lividans K+ channel. *Proc Natl Acad Sci USA* 95:6114–6117.
21. Patzlaff JS, Moeller JA, Barry BA, Brooker RJ (1998) Fourier transform infrared analysis of purified lactose permease: A monodisperse lactose permease preparation is stably folded, alpha-helical, and highly accessible to deuterium exchange. *Biochemistry* 37: 15363–15375.
22. Sayeed WM, Baenziger JE (2009) Structural characterization of the osmosensor ProP. *Biochim Biophys Acta* 1788:1108–1115.
23. Jiang X, et al. (2012) Evidence for an intermediate conformational state of LacY. *Proc Natl Acad Sci USA* 109:E698–E704.
24. Majumdar DS, et al. (2007) Single-molecule FRET reveals sugar-induced conformational dynamics in LacY. *Proc Natl Acad Sci USA* 104:12640–12645.
25. Nie Y, Sabetfard FE, Kaback HR (2008) The Cys154→Gly mutation in LacY causes constitutive opening of the hydrophilic periplasmic pathway. *J Mol Biol* 379:695–703.
26. Liu Z, Madej MG, Kaback HR (2010) Helix dynamics in LacY: Helices II and IV. *J Mol Biol* 396:617–626.
27. Smirnova IN, Kaback HR (2003) A mutation in the lactose permease of Escherichia coli that decreases conformational flexibility and increases protein stability. *Biochemistry* 42:3025–3031.
28. Ermolova NV, Smirnova IN, Kasho VN, Kaback HR (2005) Interhelical packing modulates conformational flexibility in the lactose permease of *Escherichia coli*. *Biochemistry* 44:7669–7677.
29. Zhou Y, Madej MG, Guan L, Nie Y, Kaback HR (2011) An early event in the transport mechanism of LacY protein: Interaction between helices V and I. *J Biol Chem* 286: 30415–30422.
30. Huang Y, Lemieux MJ, Song J, Auer M, Wang DN (2003) Structure and mechanism of the glycerol-3-phosphate transporter from Escherichia coli. *Science* 301:616–620.
31. Smirnova I, Kasho V, Sugihara J, Kaback HR (2011) Opening the periplasmic cavity in lactose permease is the limiting step for sugar binding. *Proc Natl Acad Sci USA* 108: 15147–15151.
32. Viitanen P, Garcia ML, Kaback HR (1984) Purified reconstituted lac carrier protein from *Escherichia coli* is fully functional. *Proc Natl Acad Sci USA* 81:1629–1633.
33. Newstead S, et al. (2011) Crystal structure of a prokaryotic homologue of the mammalian oligopeptide-proton symporters, PepT1 and PepT2. *EMBO J* 30:417–426.
34. Yin Y, He X, Szewczyk P, Nguyen T, Chang G (2006) Structure of the multidrug transporter EmrD from Escherichia coli. *Science* 312:741–744.
35. Shen MY, Sali A (2006) Statistical potential for assessment and prediction of protein structures. *Protein Sci* 15:2507–2524.
36. Warshaviak DT, Serbulea L, Houk KN, Hubbell WL (2011) Conformational analysis of a nitroxide side chain in an α-helix with density functional theory. *J Phys Chem B* 115: 397–405.
37. Langelaan DN, Wieczorek M, Blouin C, Rainey JK (2010) Improved helix and kink characterization in membrane proteins allows evaluation of kink sequence predictors. *J Chem Inf Model* 50:2213–2220.
38. Law CJ, Maloney PC, Wang DN (2008) Ins and outs of major facilitator superfamily antiporters. *Annu Rev Microbiol* 62:289–305.
39. Guan L, Weinglass AB, Kaback HR (2001) Helix packing in the lactose permease of Escherichia coli: Localization of helix VI. *J Mol Biol* 312:69–77.
40. Sahin-Toth M, Kaback HR (2001) Arg-302 facilitates deprotonation of Glu-325 in the transport mechanism of the lactose permease from *Escherichia coli*. *Proc Natl Acad Sci USA* 98:6068–6073.
41. Mitchell P (1967) Translocations through natural membranes. *Adv Enzymol Relat Areas Mol Biol* 29:33–87.
42. Menick DR, Sarkar HK, Poonian MS, Kaback HR (1985) cys154 Is important for *lac* permease activity in *Escherichia coli*. *Biochem Biophys Res Commun* 132:162–170.
43. Nie Y, Smirnova I, Kasho V, Kaback HR (2006) Energetics of ligand-induced conformational flexibility in the lactose permease of Escherichia coli. *J Biol Chem* 281: 35779–35784.
44. van Iwaarden PR, Driessen AJ, Lolkema JS, Kaback HR, Konings WN (1993) Exchange, efflux, and substrate binding by cysteine mutants of the lactose permease of Escherichia coli. *Biochemistry* 32:5419–5424.
45. Kaczorowski GJ, Robertson DE, Kaback HR (1979) Mechanism of lactose translocation in membrane vesicles from Escherichia coli. 2. Effect of imposed delta psi, delta pH, and Delta mu H+. *Biochemistry* 18:3697–3704.
46. Sali A, Blundell TL (1993) Comparative protein modelling by satisfaction of spatial restraints. *J Mol Biol* 234:779–815.
47. Altenbach C, Kusnetzow AK, Ernst OP, Hofmann KP, Hubbell WL (2008) High-resolution distance mapping in rhodopsin reveals the pattern of helix movement due to activation. *Proc Natl Acad Sci USA* 105:7439–7444.
48. Hirai T, Heymann JA, Maloney PC, Subramaniam S (2003) Structural model for 12-helix transporters belonging to the major facilitator superfamily. *J Bacteriol* 185: 1712–1718.
49. Pettersen EF, et al. (2004) UCSF Chimera—A visualization system for exploratory research and analysis. *J Comput Chem* 25:1605–1612.
50. Pintilie GD, Zhang J, Goddard TD, Chiu W, Gossard DC (2010) Quantitative analysis of cryo-EM density map segmentation by watershed and scale-space filtering, and fitting of structures by alignment to regions. *J Struct Biol* 170:427–438.